ac Josephson effects in Nb/InAs/Nb junctions with integrated resonators

K. Biedermann, A. Chrestin,* T. Matsuyama, and U. Merkt
Universität Hamburg, Institut für Angewandte Physik und Zentrum für Mikrostrukturforschung, Jungiusstraße 11, D-20355 Hamburg, Germany

(Received 9 February 2000; revised manuscript received 18 December 2000; published 20 March 2001)

Investigations of the ac Josephson effect in Nb/*p*-type InAs/Nb junctions are presented. Two distinguished features of these devices are an integrated resonator formed by the overlap of two Nb electrodes with an intermediate anodic oxide and their high characteristic voltages I_cR_N of about 1 mV. Under radio-frequency irradiation, we observe Shapiro steps whose widths follow Bessel functions for high irradiated power. Because of the integrated resonator, self-resonances of the ac Josephson effect can be studied in the current-voltage characteristics. Using a modified resistively shunted junction model which accounts for the presence of the resonator and a nonuniform lateral current distribution, we can describe the magnetic-field dependence of the resonance amplitude. A resonance is also observed when the Josephson frequency is exactly half the lowest resonance frequency, which is beyond the simple model. A possible explanation is provided by a nonsinusoidal current-phase relation established under nonequilibrium conditions.

DOI: 10.1103/PhysRevB.63.144512 PACS number(s): 74.50.+r, 74.80.Fp

I. INTRODUCTION

The experimental and theoretical study of the ac Josephson effect in weak links has attracted much interest in recent years.[1,2] One experimental goal is to use the junctions as local oscillators in the GHz range. Some authors[3] use long Josephson junctions, so-called flux-flow oscillators, whose current-voltage characteristics are determined by vortex motion.[4,5] The most common approach is to build arrays of junctions to reach high power levels of the emitted radiation. A severe problem of this approach is that the junctions have to radiate phase coherently. The high I_cR_N products[6] of the critical current I_c and the normal resistance R_N in our junctions of about 1 mV correspond to an estimated power level on the order of 1 μW. This encourages us to investigate their potential as single-junction sources for the investigation of other mesoscopic devices,[7,8] thus avoiding the coherence problem. The reason for the high I_cR_N product is the absence of a Schottky barrier between the contact of *p*-type InAs and the superconducting metal Nb as well as nearly matched Fermi velocities, which results in highly transmissive interfaces.[9]

The radio-frequency (rf) radiation from the ac Josephson effect at finite voltages between the superconducting electrodes is emitted into the resonator formed by the overlap of two Nb electrodes with an anodic oxide as a dielectric. Sharp structures are observed in the derivatives of the current-voltage characteristics at voltages where the Josephson frequency corresponds to a cavity resonance. Weak links usally do not form resonators, however, for weak links resonances are observed in point contacts[10] or microbridges[11] when they are connected to an external cavity. A theory for these so-called Fiske steps[12] or self-resonances has been developed by Kulik.[13] Eck, Scalapino, and Taylor report on a resonance in the current-voltage characteristic when the phase velocity associated with the current-density distribution matches the phase velocity of the electromagnetic fields.[14] In both references, a homogeneous current distribution over the whole two-dimensional area of a Josephson tunnel junction was considered. In our device we have to take into account that the current is concentrated only at one edge of the resonator. Moreover, we have found that the current is inhomogeneously distributed across the junction width in our junctions. Both nonuniformities are contained in our modification of the Kulik model. It is well known that inhomogeneities of the current distribution result in a finite resonance amplitude even at zero applied magnetic field,[15,16] whereas a finite field is necessary to excite the resonances in the homogeneous case.[17,18] In addition to the peaks at Josephson frequencies corresponding to cavity resonances, for the first time we observe a peak at half the lowest resonance frequency in such junctions.

This paper is organized as follows. In Sec. II we describe the preparation of our devices and experimental details of the measurements. The magnetic-field dependence of the amplitude of the Fiske resonances is described in an adopted resistively shunted junction (RSJ) model evaluated in Sec. III. This model takes into account the integrated resonator and is valid for arbitrary current distributions. In Sec. IV we study the power dependence of the widths of the Shapiro steps and compare the measured amplitudes of the Fiske resonances with the ones of the RSJ model. A rather good agreement for the integer resonances is achieved. Additionally, we discuss a possible extension of the model to explain the observed half-integer resonance.

II. EXPERIMENTAL DETAILS

A schematic view of our junctions is depicted in Fig. 1(a). The (100)-oriented InAs wafers are Zn doped with a concentration of about 2×10^{17} cm^{-3}. Mechanical and chemical polishing is important to achieve a surface smoothness in the nm range, which is necessary for high-quality interfaces between InAs and Nb. After the definition of the resist mask of the lower Nb electrode by conventional photolithography, the first Nb film with thickness $t=90$ nm is magnetron sputtered in an Ar plasma at a pressure of 10^{-2} mbar. Two separate *in situ* cleaning steps prior to the electrode deposi-

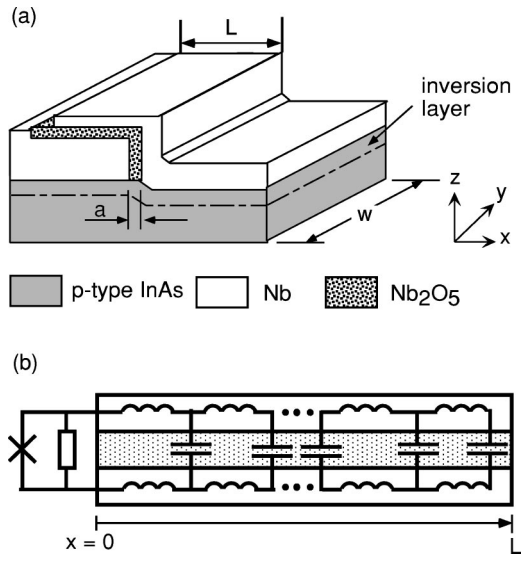

FIG. 1. (a) Schematic view of the Nb/*p*-type InAs(2DES)/Nb junction. The resonator is built by the overlap of length L and width w of the two Nb electrodes with the anodic oxide Nb_2O_5 in between. (b) Equivalent electronic circuit for the junction in our adopted RSJ model. The cross denotes the Josephson junction, and the resistor stands for the quasiparticle current. The resonator is modeled by an LC network.

tion are important to clean the target and to remove oxides from the InAs surface, respectively. The electrode patterning is completed by a lift-off process. After this lift-off step the Nb electrode is anodically oxidized at one end.[19] The oxide thickness $a \geqslant 10$ nm defines the channel length and is controlled during the anodization by the applied voltage, 1 V corresponding to 2 nm Nb_2O_5. Hence, with this method channel lengths in the nanometer range are easily achieved. After the oxidation process the oxidized InAs is removed by wet etching in a 1:1 H_2SO_4:H_2O solution in order to facilitate a good contact between the two-dimensional electron system (2DES) in the inversion layer on the InAs and the second Nb electrode. This electrode is defined and deposited in the same way as described above. The two Nb electrodes are insulated by the intermediate anodic oxide[20] overlapping along a length $L \approx 3$ μm. The junction widths w in the samples presented here are 10 and 20 μm. We have studied additional junctions with widths up to 91 μm which all show qualitatively the same behavior. All geometrical quantities are read from scanning-electron microscopy (SEM) and atomic-force microscopy (AFM) images.

The measurements are performed in a liquid-helium cryostat at temperatures down to 1.5 K. Leads are filtered at room temperature with commercially available fed-through capacitors. All measurements are done in a four-probe setup under current bias conditions. In measurements with rf irradiation ($\nu \cong 15$ GHz) a cryoperm tube is used for sample shielding and the wave is guided to the sample through a coaxial brass waveguide terminated by an antenna. The differential resistance is measured by standard lock-in techniques with a modulating current of 1 μA at a frequency of 300 Hz.

III. RSJ MODEL WITH RESONATORS

Josephson junctions are often described by the resistively shunted junction model.[21] The total dc current at a finite voltage is given by the sum of the time-averaged ac Josephson current and the quasiparticle current through a resistor. In the voltage bias case the time averaged ac Josephson current is zero. In the current bias case or if any frequency dependent elements are present the situation is different. Hence, we assume a nonzero but small time-averaged ac Josephson current $\overline{I_s}$ with $|\overline{I_s}| \ll I_c$. A corresponding RSJ model was first considered by Forder.[22] Here, we apply his results to our specific junction geometry. In Fig. 1(b) the equivalent electric circuit is depicted. In contrast to Forder, we have to take into account the geometry of the junction to deal with its interaction with the spatially extended eigenmodes of the resonator.[23] As it is clear from Fig. 1(a) the Josephson current flows only at one end of the resonator. This is different from the rigorously studied case of junctions where the two-dimensional junction area itself forms the resonator. Consequently, we use a one-dimensional current density J over the width w of the junction. According to our assumption, we are close to the voltage bias case, where the phase difference across the Josephson junction varies as $\phi(y,t) = \omega_J t + \pi/2 - ky$.[22] The Josephson frequency $\omega_J = (2e/\hbar)\overline{V}$ is given by the dc bias voltage $\overline{V}$ across the junction. The y dependence results from a vertically applied magnetic field producing a flux Φ through the junction; $k = 2\pi\Phi/(\Phi_0 w)$ with the magnetic flux quantum $\Phi_0 = h/2e$. To account for the finite time average $\overline{I_s}$ of the ac Josephson current, we allow for a small phase perturbation $\phi_1(y,t) = \mathrm{Im}[\varphi_1(y)\exp(i\omega t)]$, $|\phi_1| \ll |\phi|$. It corresponds to a voltage perturbation $V_1(y,t) = (\hbar/2e)\dot{\phi}_1(y,t)$. Thus, beside the unperturbed supercurrent density $J_{s0} = J_c \sin\phi$ with vanishing time average we find a current component $J_{s1} = J_c \phi_1 \cos\phi$ yielding the desired finite time average of the supercurrent density

$$\overline{J_s} = \overline{J_{s1}} = -\tfrac{1}{2} J(y)\,\mathrm{Im}[i\varphi_1(y)\exp(iky)]. \tag{1}$$

We want to consider junctions with a position-dependent critical current, i.e., a nonhomogeneous current distribution over the junction width w. Therefore, we replaced J_c by $J(y)$ in Eq. (1). The electromagnetic field excited by the Josephson radiation within the resonator leads to a modulation of the phase perturbation $\phi_1(x,y,t)$ over the whole resonator area, which has to be determined to find its influence on the Josephson junction at $x = 0$ [see Fig. 1(b)]. The wave equation

$$\frac{\partial^2\phi_1}{\partial x^2} + \frac{\partial^2\phi_1}{\partial y^2} - \frac{1}{c'^2}\left(\frac{\partial^2\phi_1}{\partial t^2} + \frac{\sigma}{\epsilon_r\epsilon_0}\frac{\partial\phi_1}{\partial t}\right) = 0 \tag{2}$$

for ϕ_1[18] has to be solved with the boundary conditions

$$\left.\frac{\partial\phi_1}{\partial x}\right|_{x=0} = \frac{J(y)}{\delta_J}\cos(\omega t - ky) + \frac{1}{\gamma c'}\left.\frac{\partial\phi_1}{\partial t}\right|_{x=0},$$

$$\left.\frac{\partial\phi_1}{\partial y}\right|_{y=0} = \left.\frac{\partial\phi_1}{\partial y}\right|_{y=w} = 0,$$

$$\left.\frac{\partial\phi_1}{\partial x}\right|_{x=L} = 0. \tag{3}$$

These boundary conditions express the fact that the current flows out of the resonator at $x=0$, where the junction is located. In Eqs. (2) and (3), we have introduced the dielectric constant ϵ_r of the oxide, the phase velocity $c' = [a/(\epsilon_r d)]^{1/2}\cdot c$ in the resonator,[24] where c denotes the speed of light, $\gamma = r/(\mu_0 d c')$ the ratio of the specific resistance r of the junction and the wave impedance $z_w = \mu_0 d c'$ of the resonator, and $\delta_J = [(2e/\hbar)\mu_0 d]^{-1}$. The length $d = a + 2\lambda\coth(t/\lambda)$ denotes the ''magnetic thickness'' of the resonator,[25] determined by the oxide thickness a, the thickness t of the superconducting films, and the penetration depth λ. The conductivity $\sigma \propto Q^{-1}$ represents losses in the dielectric, and Q is the quality factor of the resonator. Employing the ansatz

$$\varphi_1(x,y) = \sum_{n=0}^{\infty} a_n \cos(\kappa_n[x-L])\cos(n\pi y/w) \tag{4}$$

we can solve the differential equation. By inserting it into Eq. (1), the dc component of the supercurrent

$$\overline{I_S} = -\frac{1}{2}\int_0^w J(y)\,\mathrm{Im}[i\varphi_1(0,y)\exp(iky)]dy,$$

$$= \frac{\gamma c' w}{2\delta_J \omega}\sum_{n=0}^{\infty}\frac{F_n^2(k)}{2-\delta_{n,0}}\mathrm{Re}\left[\frac{1}{1+i(\gamma c'/\omega)\kappa_n\tan(\kappa_n L)}\right] \tag{5}$$

is found, where $\kappa_n = (1-(\omega_{\mathrm{res}}/\omega)^2 - i/Q)^{1/2}\cdot\omega/c'$. This expression describes a series of peaklike contributions to the current at voltages when the Josephson frequency $\omega_J = (2e/\hbar)\overline{V}$ corresponds to one of the cavity resonances

$$\omega_{\mathrm{res}} = \pi c' \sqrt{\frac{n^2}{w^2} + \frac{m^2}{L^2}}, \tag{6}$$

with n and m being integers. The magnetic-field dependence is given by

$$F_n^2(k) = B_n^2(k) + C_n^2(k),$$

$$B_n(k) = \frac{2-\delta_{n,0}}{w}\int_0^w J(y)\cos(ky)\cos(n\pi y/w)dy,$$

$$C_n(k) = \frac{2-\delta_{n,0}}{w}\int_0^w J(y)\sin(ky)\cos(n\pi y/w)dy, \tag{7}$$

where δ_{nm} is the Kronecker symbol. For a given current distribution $J(y)$ along the junction width, we can calculate from Eq. (7) the amplitude variation of each resonance when the strength of the applied magnetic field changes. Note that it only depends on the ''transverse'' index n because of the one-dimensional nature of our junction model.

IV. EXPERIMENTAL RESULTS: SHAPIRO STEPS AND FISKE RESONANCES

Under external rf irradiation a Josephson junction shows steps in the resistive branch of its current-voltage characteristic. These Shapiro steps[26] appear when the Josephson frequency ω_J equals an integer multiple of the irradiated frequency ω_{rf}. In Fig. 2(a) current-voltage characteristics are shown for different rf power as well as without irradiation, and in Fig. 2(b) a current-voltage characteristic and its derivative are depicted. Obviously, the Shapiro steps appear at voltages $V_n = \pm n\cdot(2e/\hbar)\omega_{\mathrm{rf}}$ which correspond to the irradiated frequency of 15 GHz and their widths modulate with the rf power. The $I_c R_N$ product of 640 μV is smaller than our best values that exceed 1 mV. The reason is the relatively large oxide thickness $a = 120$ nm of this particular junction that already approaches the coherence length of the semiconductor[9] and thus leads to a weaker coupling between the two superconductors. The excess current of this sample $I_{\mathrm{exc}} = 162$ μA exceeds its critical current $I_c = 80$ μA by a factor of 2. This ratio is typical for our junctions. Distinct steps are observed in the direct and even more clearly in the differential characteristic at voltages which correspond to the irradiated frequency of 15 GHz. In Fig. 2(c) the critical current I_c and the widths of the first four steps are shown as a function of the irradiated rf power. As expected from standard theory[18] the step widths and the critical current modulate with the rf power. We plot the step widths against the square root of the nominally irradiated power since the rf current cannot be measured directly. The solid lines are the expected Bessel functions $\mathcal{J}_n$ of order n, which for high rf currents fit the measured data very well. Our junctions are current biased because the impedance of the electronical environment is much larger than the one of the junction. Despite this fact, the step widths follow the well-known relation

$$\Delta I = I_c\cdot\left|\mathcal{J}_n\left(\frac{V_{\mathrm{rf}}}{V_{\mathrm{dc}}}\right)\right| \tag{8}$$

of the voltage bias case.[18] Here, we have the ac voltage V_{rf} over the contact and the dc voltage position V_{dc} of the step. For the calculations in Fig. 2(c) we have used the relation

$$\Delta I = k_1\cdot|\mathcal{J}_n(k_2\cdot i_{\mathrm{rf}})|. \tag{9}$$

The current i_{rf} is taken as the square root of the irradiated power and $k_{1,2}$ are fit parameters. The fits of all steps in Fig. 2(c) are done with one set of parameters $k_{1,2}$. Comparison of Eqs. (8) and (9) yields a constant $k_1 = 24.7$ μA which is much smaller than the critical current $I_c = 80$ μA in the absence of rf radiation. A possible explanation of this difference could be the fact that our junctions are current biased. For tunnel junctions very successful models exist that de-

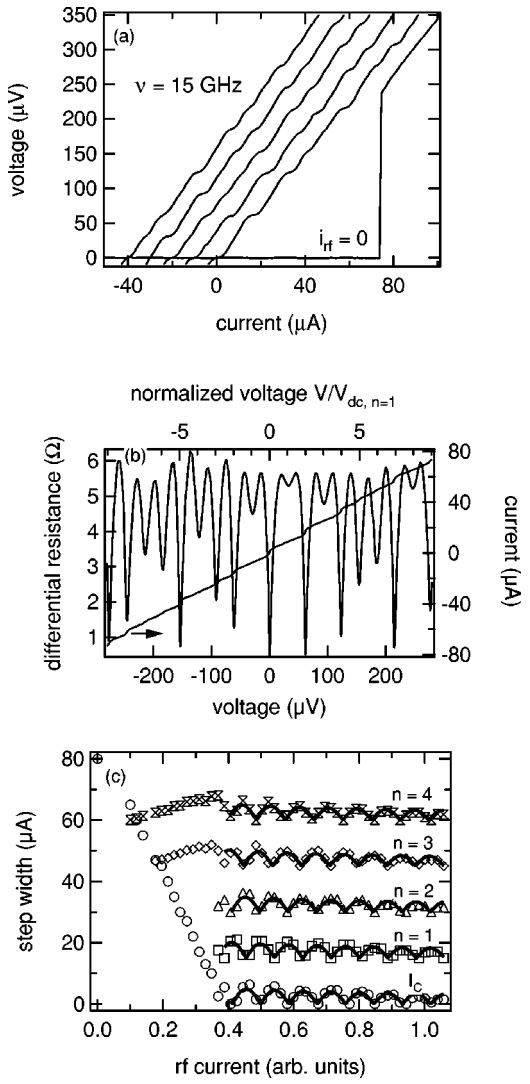

FIG. 2. (a) Direct current-voltage characteristics for different rf powers. Traces from right to left are measured without rf, 0.165, 0.182, 0.198, 0.216, and 0.233 mW, respectively. The curves for rf powers larger than 0.182 mW are successively shifted by -10 μA. (b) Direct and differential current-voltage characteristic at 1.7 K and nominal power 0.165 mW. (c) Step width of the critical current and of the first four Shapiro steps as a function of the rf current. The curves are successively offset by 15 μA. The solid lines describe corresponding Bessel functions. The upper voltage axis is divided by the voltage $V_{\mathrm{dc},n=1}=(2e/\hbar)\omega_{\mathrm{rf}}=31$ μV.

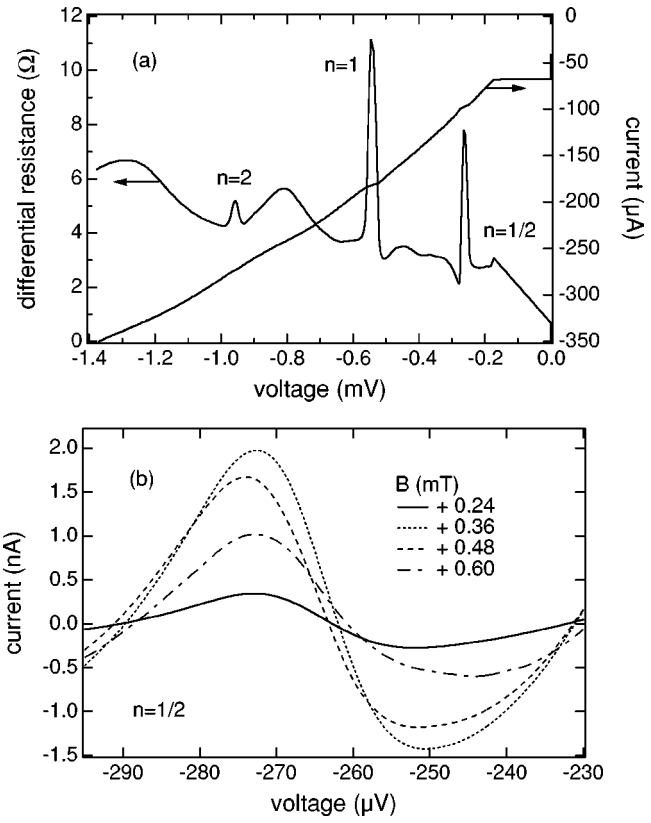

FIG. 3. (a) Direct and differential current-voltage characteristic at 2.2 K. The sharp structures in the differential curve are Fiske resonances due to the integrated resonator. (b) Direct characteristics in the region of the $n=1/2$ resonance for various strengths of the applied magnetic field. The step amplitude is the difference between respective maximum and minimum.

scribe the current bias case.[27,28] For weak links with a finite normal conductivity the situation becomes more complicated because nonequilibrium effects appear as discussed below. Another reason for the observed deviation might be the presence of an excess current in our junctions.

In Fig. 3(a) the negative branches of the direct and differential current-voltage characteristic of a junction with a width $w=20$ μm are shown. The three sharp structures at voltages 0.26, 0.56, and 0.96 mV are Fiske- or self-resonances. These resonances occur when the Josephson frequency ω_J is equal to one of the frequencies ω_{res} of Eq. (6) which describes longitudinal and transversal resonances as well as mixed modes. Because the overlap is just $L=3$ μm, the longitudinal resonances occur at higher voltages and we measure only transversal ($m=0$) Fiske resonances in this sample. In junctions with longer overlap we observe also longitudinal ($m\neq 0$) and mixed ($m\neq 0$, $n\neq 0$) resonances with voltage positions again given by Eq. (6). We find that Eq. (6) holds for all our junctions with different overlap lengths L, widths w, and channel lengths a.[23,29] From the dimensions $L=3$ μm and $w=20$ μm of the resonator of the sample in Figs. 3(a) and 3(b) we find for the lowest resonance frequency ($n=1$, $m=0$) $\omega_{\mathrm{res}}=1.76$ GHz corresponding to a voltage 0.57 mV. Here, the oxide thickness $a=10$ nm and the thickness of the Nb electrodes $t=90$ nm are taken from AFM images. For the penetration depth λ values between $\lambda=86$ nm (Ref. 30) and $\lambda=122$ nm (Ref. 31) are found in the literature. The actual magnitude depends on the scattering length in the Nb electrodes. We use a value $\lambda=90$ nm in the calculation of the resonance frequencies ω_{res}. The resonance at the voltage 0.26 mV corresponds to $n=1/2$ and will be discussed further at the end of this section. Note that even when the uncertainties of all geometrical quantities are accounted for, the lowest observed resonance at 0.26 mV cannot be related to an index $n=1$. From the experimental traces of the differential resistance we evaluate a step amplitude by inverting the differential characteristic around the resonance and integrating it over the voltage. Be-

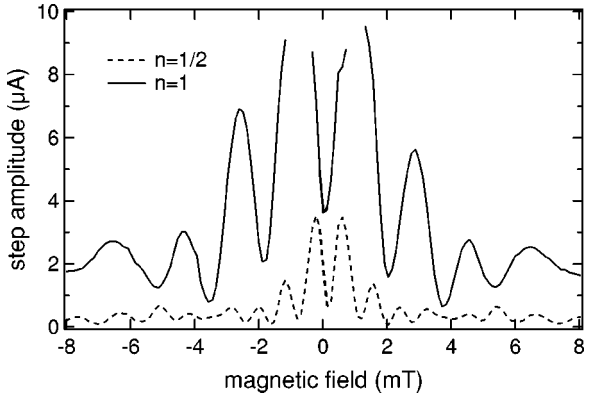

FIG. 4. Magnetic-field dependence of the step amplitude of the $n=1/2$ (dashed line) and $n=1$ (solid line) Fiske resonance. The $n=1$ resonance exhibits twice the period of the $n=1/2$ resonance. The magnetic field is applied parallel to the current direction.

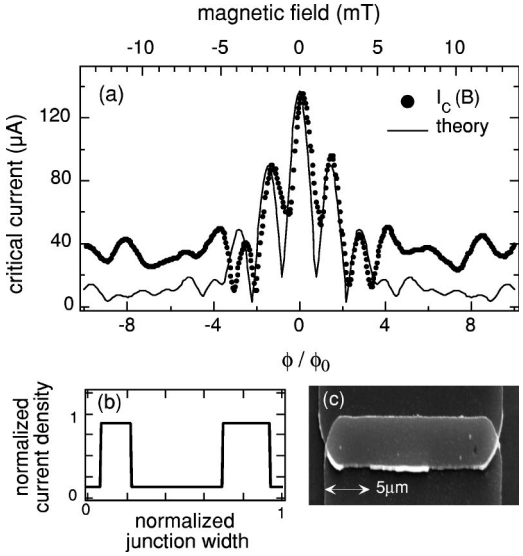

FIG. 5. (a) Fraunhofer pattern at 2.2 K with the magnetic field applied parallel to the junction in current direction. The dots are measured data. The solid line is calculated after Barone (Ref. 18) with the current distribution shown in (b). (c) SEM picture of the overlap of the two Nb electrodes motivating the current distribution in (b).

fore the integration we subtract a polynomial of second order to take into account the background which results from the additional conductivity due to multiple Andreev reflection.[32,33] The resulting curves for the $n=1/2$ resonance are shown in Fig. 3(b) for different strengths of the magnetic field applied in parallel to the current flow. This is the most stable configuration against magnetic-flux penetration. The model of Sec. III is valid as long as the applied magnetic field yields a phase modulation along the junction width, i.e., the magnetic field must be applied perpendicular to it.

The step amplitude of a Fiske resonance is taken as the difference between maximum and minimum in the numerically reconstructed current-voltage characteristic. As expected, the step amplitude modulates with the strength of the applied magnetic field. The step amplitudes for the $n=1/2$ and $n=1$ resonance versus the magnetic-field strength are shown in Fig. 4. We find that the $n=1$ resonance has twice the period in a magnetic field compared to the resonance tentatively labeled as $n=1/2$. The period of the $n=1$ resonance of about 1.5 mT is equal to the one of the corresponding Fraunhofer pattern. From Eq. (7) we expect a vanishing step amplitude at $B=0$ for a homogeneous current distribution across the junction width, contrary to our observation. However, if we assume that the current is inhomogeneously distributed as shown in Fig. 5(b), the magnetic-field dependence of the step amplitude obtained from Eq. (7) fits qualitatively well with the experimental data (see dashed line in Fig. 6). Obviously, the homogeneous distribution (see dotted line in Fig. 6) yields a much worse fit. With the same current distribution, we also can reproduce quite well the magnetic-field dependence of the critical current as shown in Fig. 5(a).[18] A direct calculation of the current distribution from the measured Fraunhofer pattern is not possible due to the not single-valued phase information.[34] The assumed current distribution is motivated by the SEM image in Fig. 5(c). It shows the overlap of the two Nb electrodes. The white regions are bent Nb edges providing a weaker coupling and therefore a reduced current density compared to the other regions. We have also calculated the step amplitude for the $n=2$ resonance and have compared it with the measured data. The agreement is as good as for the Fraunhofer pattern and the $n=1$ resonance.

As depicted in Fig. 4 we measure a half integer self-resonance corresponding to $n=1/2$. Other authors also have observed half-integer effects by using an external irradiation method.[35,36] The appearance of the $n=1/2$ resonance cannot be explained in the RSJ approach of Sec. III. In fact, it is well known that weak links can show considerable deviations from the RSJ model.[21] A possible explanation might be a strong deviation of the phase dependence of the critical current from $\sin\phi$ behavior in the nonequilibrium state (V

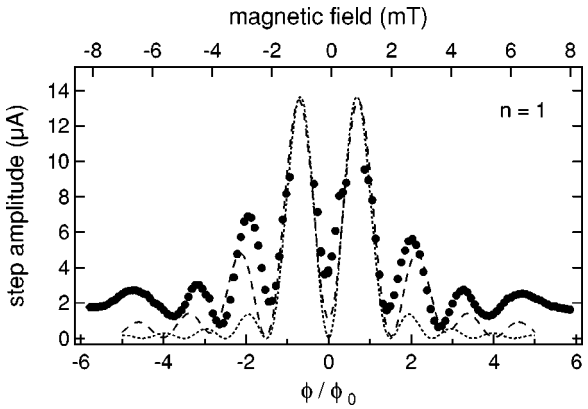

FIG. 6. Magnetic-flux dependence of the first integer Fiske resonance ($n=1$) at 2.2 K with the magnetic field applied parallel to the junction. The dashed curve is the magnetic-field dependence of the step amplitude $F_1^2(k)$ of our adopted RSJ model with the current distribution of Fig. 5(b). It agrees much better with the measured data than the amplitude $F_1^2(k)$ calculated with a uniform current distribution (dotted line).

$\neq 0$) of these junctions. The appearance of nonsinusoidal current-phase relations in such Josephson junctions due to nonequilibrium is in fact a research field of topical interest.[35,37] For example the authors of Ref. 35 explain the appearance of a half-integer Shapiro step by the existence of nonequilibrium, which is described by a theory of Argaman.[38] Here, as well as in other publications, e.g., of Octavio, Skopcol, and Tinkham,[39] nonequilibrium effects are observable depending on the ratio of the relaxation time of the quasiparticles and the time of a Josephson oscillation. If we assume such a strong component proportional to $\sin(2\phi)$ and write $J_s = J_a \sin\phi + J_b \sin(2\phi)$, we obtain a set of two coupled differential equations in the approach of Sec. III. This cannot be solved easily, but it is clear that it will result in the appearance of a resonance peak at $\omega = \omega_{\rm res}$, where the resonance frequency $\omega_{\rm res}$ is obtained for $n = 1/2$ from Eq. (6). Moreover, this resonance will have half the period of the $n = 1$ resonance in an external magnetic field as it is observed experimentally in Fig. 4. The existence of a $\sin(2\phi)$ current component also leads to half-integer Shapiro steps. Indeed we observe half-integer Shapiro steps up to the order $n = 7/2$ along with a half-integer Fiske resonance corresponding to $n = 1/2$ in Fig. 7. On the other hand, a $\sin(2\phi)$ component of the critical current of considerable strength is not resolved in our measurement of the magnetic-field dependence of the critical current. This is consistent with the fact that only at finite voltages nonequilibrium effects are expected.[38] The appearance of nonequilibrium depends on the relation between the time of a Josephson oscillation and the characteristic relaxation time τ_e. In the theory of Argaman[38] the maximum voltage for which nonequilibrium effects should occur can be estimated by $V_{\rm NEQ} = \hbar/(2e\tau_e)$. Here, τ_e can be estimated[35] from the number of multiple Andreev reflections times the transit time τ_d of an electron through the barrier. This transit time depends on the Thouless energy $E_{\rm Th} = \hbar/\tau_d$.[29] We obtain $V_{\rm NEQ} = 360\ \mu$V for our samples. In fact, for a wider junction of width $w = 91\ \mu$m we observe a Fiske resonance corresponding to $n = 3/2$ at a voltage $V = 236\ \mu$V. Clearly, further research is necessary to achieve a better understanding of the nature of the half-integer resonances in the ballistic regime of weak links.

V. CONCLUSIONS

We have prepared Nb/*p*-type InAs (2DES)/Nb junctions with an integrated microwave resonator. This resonator makes the junctions especially interesting for investigations of the ac Josephson effect in weak links on semiconductors. Under irradiation we observe Shapiro steps in the current-voltage characteristics. The step width modulates with the irradiated power roughly as expected for the voltage bias case. Due to the integrated resonator our junctions show Fiske resonances. Their voltage positions and their magnetic-field dependencies can be understood in a modified RSJ model, which takes into account the integrated resonator and is valid for arbitrary current distributions along the channel of the 2DES. In addition, we have observed a resonance whose voltage position corresponds to $n = 1/2$, i.e., a resonance with half the period compared to the corresponding Fraunhofer pattern. This behavior can be explained by adding a $\sin(2\phi)$ term in the first Josephson equation to account for the presence of a nonequilibrium situation.

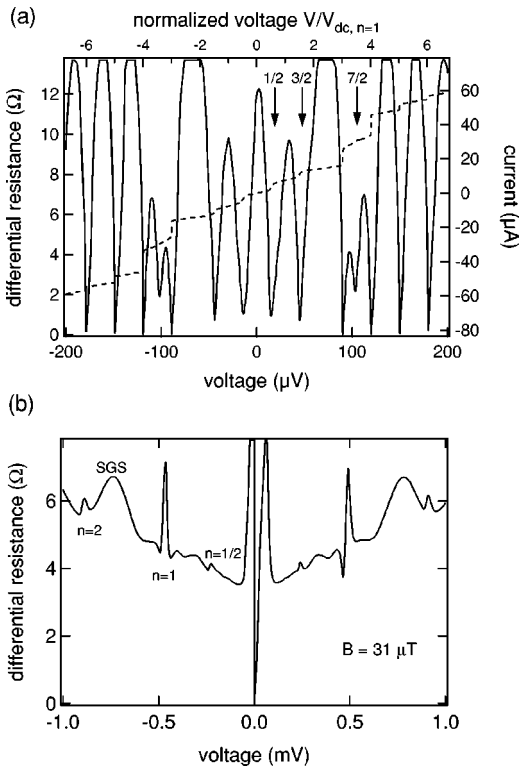

FIG. 7. (a) Direct (dashed line) and differential (solid line) current-voltage characteristic of another sample of width 20 μm under irradiation of rf (14.4 GHz). Half-integer Shapiro steps up to the order $n = 7/2$ are observed. (b) Differential current-voltage characteristic of the sample in the absence of irradiation with a half-integer Fiske resonance $n = 1/2$. The magnetic field is applied perpendicular to the current flow.

ACKNOWLEDGMENT

We thank the Deutsche Forschungsgemeinschaft for financial support via the Sonderforschungsbereich 508 ''Quantenmaterialien.''

*Present address: Siemens AG, Machtlfingerstr. 1, D-81359 München, Germany.

[1] D. Averin and A. Bardas, Phys. Rev. Lett. **75**, 1831 (1995).
[2] B. J. van Wees and H. Takayanagi, *Mesoscopic Electron Transport* (Kluwer, Dordrecht, 1996).
[3] S. V. Shitov, A. V. Ustinov, N. Iosad, and H. Kohlstedt, J. Appl. Phys. **80**, 7134 (1996).
[4] A. Davidson and N. F. Pedersen, Appl. Phys. Lett. **60**, 2017 (1992).
[5] M. V. Krasnov, V. A. Oboznov, and N. F. Pedersen, Phys. Rev. B **55**, 14 486 (1997).
[6] A. Chrestin and U. Merkt, Appl. Phys. Lett. **70**, 3149 (1997).
[7] S. Feng and Q. Hu, Phys. Rev. B **48**, 5354 (1993); Semicond. Sci. Technol. **11**, 1888 (1996).

[8] A. W. Holleitner, H. Qin, F. Simmel, B. Irmer, R. H. Blick, J. P. Kotthaus, A. V. Ustinov, and K. Eberl, New J. Phys. **2**, 1 (2000).
[9] H. Takayanagi and T. Kawakami, Phys. Rev. Lett. **54**, 2449 (1985).
[10] S. I. Bondarenko, I. M. Dmitrienko, and T. P. Narbut, Fiz. Tverd. Tela (Leningrad) **14**, 354 (1972) [Sov. Phys. Solid State **14**, 295 (1972)].
[11] V. M. Dmitriev, E. V. Kristenko, and A. L. Solovev, Phys. Status Solidi A **19**, K157 (1973).
[12] M. D. Fiske, Rev. Mod. Phys. **36**, 221 (1964).
[13] I. O. Kulik, Zh. Éksp. Teor. Fiz. **37**, 157 (1967) [Sov. Phys. JETP **12**, 111 (1967)].
[14] R. E. Eck, D. J. Scalapino, and B. N. Taylor, Phys. Rev. Lett. **13**, 15 (1964).
[15] M. Russo and R. Vaglio, Phys. Rev. B **17**, 2171 (1978).
[16] U. Gambardella, G. Celentano, V. Boffa, and S. Pace, J. Appl. Phys. **84**, 5363 (1998).
[17] M. A. H. Nerenberg and P. A. Forsyth, Jr., J. Appl. Phys. **47**, 4148 (1976).
[18] A. Barone and G. Paterno, *Physics and Applications of the Josephson Effect* (Wiley, New York, 1982).
[19] H. Kroger, L. N. Smith, and D. W. Jillie, Appl. Phys. Lett. **39**, 280 (1981).
[20] A. Chrestin, T. Matsuyama, and U. Merkt, Phys. Rev. B **55**, 8457 (1997).
[21] K. K. Likharev, Rev. Mod. Phys. **51**, 101 (1979).
[22] P. W. Forder, J. Phys. D **10**, 1413 (1977).
[23] A. Chrestin, Ph.D. thesis, Universität Hamburg, Shaker, Aachen, 1996.
[24] J. C. Swihart, J. Appl. Phys. **32**, 461 (1961).
[25] M. Weihnacht, Phys. Status Solidi **32**, K169 (1969).
[26] S. Shapiro, Phys. Rev. Lett. **11**, 80 (1963).
[27] N. R. Werthamer, Phys. Rev. **147**, 255 (1966).
[28] A. I. Larkin and Yu. N. Ovchinnikov, Zh. Éksp. Teor. Fiz. **51**, 1535 (1966) [Sov. Phys. JETP **24**, 1035 (1966)].
[29] K. Biedermann, Ph.D. thesis, Universität Hamburg, Shaker, Aachen, 2000. This thesis is available from the author on request.
[30] R. F. Broom, J. Appl. Phys. **47**, 5432 (1976).
[31] K. Schwidtal, J. Appl. Phys. **43**, 202 (1972).
[32] T. M. Klapwijk, G. E. Blonder, and M. Tinkham, Physica B & C **109&110B**, 1657 (1982).
[33] A. F. Andreev, Zh. Éksp. Teor. Fiz. **46**, 1823 (1964) [Sov. Phys. JETP **19**, 1228 (1964)].
[34] O. Nesher and E. N. Ribak, Appl. Phys. Lett. **71**, 1249 (1997).
[35] K. W. Lehnert, N. Argaman, H.-R. Blank, K. C. Wong, S. J. Allen, E. L. Hu, and H. Kroemer, Phys. Rev. Lett. **82**, 1265 (1999).
[36] H. Drexler, J. G. E. Harris, E. L. Yuh, K. C. Wong, S. J. Allen, E. G. Gwinn, H. Kroemer, and E. L. Hu, Surf. Sci. **361/362**, 306 (1996).
[37] J. J. A. Baselmans, A. F. Morpurgo, B. J. van Wees, and T. M. Klapwijk, Nature (London) **397**, 43 (1999).
[38] N. Argaman, Superlattices Microstruct. **25**, 861 (1999).
[39] M. Octavio, W. J. Skocpol, and M. Tinkham, Phys. Rev. B **17**, 159 (1978).